ISTP

RESEARCH ARTICLE

Dynamical Modeling and Dynamic Characteristics Analysis of a Coaxial Dual-Rotor System

Yubin Yue,[1,2] **Hongjun Wang,**[1,2,3,4] **and Shenglun Zhang**[2]

[1]China Academy of Machinery Science and Technology Group Co., Ltd., Beijing, China

[2]School of Mechanical and Electrical Engineering, Beijing Information Science and Technology University, Beijing, China

[3]Key Laboratory of Modern Measurement and Control Technology, Ministry of Education, Beijing Information Science and Technology University, Beijing, China

[4]Beijing International Science and Technology Cooperation Base of High-end Equipment Intelligent Perception and Control, Beijing Information Science and Technology University, Beijing, China

Abstract: The dual-rotor structure serves as the primary source of vibration in aero-engines. Understanding its dynamical model and analyzing dynamic characteristics, such as critical speed and unbalanced response, are crucial for rotor system dynamics. Previous work introduced a coaxial dual-rotor-support scheme for aero-engines, and a physical model featuring a high-speed flexible inner rotor with a substantial length-to-diameter ratio was designed. Then a finite element (FE) dynamic model based on the Timoshenko beam elements and rigid body kinematics of the dual-rotor system is modeled, with the Newmark method and Newton–Raphson method used for the numerical calculation to study the dynamic characteristics of the system. Three different simulation models, including beam-based FE (1D) model, solid-based FE (3D) model, and transfer matrix) model, were designed to study the characteristics of mode and the critical speed characteristic of the dual-rotor system. The unbalanced response of the dual-rotor system was analyzed to study the influence of mass unbalance on the rotor system. The effect of different disk unbalance phases and different speed ratios on the dynamic characteristics of the dual-rotor system was investigated in detail. The experimental result shows that the beam-based FE model is effective and suitable for studying the dual-rotor system.

Keywords: coaxial dual-rotor system; dynamical modeling; dynamic characteristics analysis; rotor dynamics

I. INTRODUCTION

Modern aero-engine and gas turbines usually adopt the structure of a dual-rotor system, which consists of many rotary and stationary accessories. The dual-rotor structure contains many exciting forces and has complex dynamic behaviors. Therefore, it is crucial to establish an appropriately simplified dynamic model according to the double-rotor system's structure and working characteristics. Meanwhile, it is also essential to solve the dynamic differential equation of the dual-rotor system. Modern numerical calculation methods of rotor dynamics are mainly included in the finite element (FE) method and the transfer matrix (TM) method [1,2].

Ruhl *et al.* [3] derived an impedance matrix between the bearing support structure forces and the corresponding displacements, matched with the FE model of the turbo rotor system. Nelson *et al.* [4] developed a rotor-bearing system that used the FE method to establish formulae, including rotational inertia, gyroscopic moment, and axial load. Hibner *et al.* [5] have applied the TM method to the two-shaft aircraft to introduce the multi-shaft critical speeds and nonlinear damped response. Wang *et al.* [6] developed a one-dimensional Timoshenko beam-type model and a three-dimensional model for a dual-rotor system with inter-shaft bearing to analyze the dynamic of the dual-rotor

system. Wang *et al.* [7] established a new dynamic model of the dual-rotor system's rubbing fault and applied the numerical integration method to obtain the system's dynamic behavior. Wang *et al.* [8] solved the governing equations of the dual-rotor system with unbalanced–misalignment coupling faults by the Runge–Kutta method. Wang *et al.* [9] built a FE model of a dual-rotor-support-casing system with an unbalanced and time-varying pulse load to analyze the vibration features of the system. Wang *et al.* [10] presented the governing equations of motion of the rod fastening rotor system using the FE method based on Timoshenko beam theory. Wang *et al.* [11] proposed a typical rod fastening rotor model to study the nonlinear dynamic characteristics, confirming that the unbalanced magnitude and phase difference are critical systems response parameters. Jalali *et al.* [12] carried out a dynamic analysis of a high-speed rotor with specific geometrical and mechanical properties by using a 3D FE model, one-dimensional beam-type model, and experimental modal test. Yang *et al.* [13] established a dynamical model based on the TM method based on a gas turbine rotor system and solved the natural vibration characteristics. Yang *et al.* [14] modeled a dual-rotor-bearing double casing system to study the vibration behaviors with pedestal looseness and rotor–stator rub. Yang *et al.* [15] utilized the Euler–Bernoulli beam to establish a double-disk rotor system and studied the influence of speed and unbalanced phase difference on vibration response. Fei [16] presented a FE model of

---

Corresponding author: Hongjun Wang (e-mail: wanghj_bistu@163.com).

dual-rotor systems and developed its solution method to calculate the dynamics. Lu *et al.* [17] built a simplified dynamic model of a dual-rotor system coupled with a bladed disk and analyzed the blade's impact on the critical speed and other dynamic characteristics. Jin *et al.* [18] designed a dual-rotor experimental rig according to a dual-rotor aero-engine and established the dynamic model of the dual-rotor-bearing system of the test rig based on the FE method. According to the FE approach, Zhang *et al.* [19] acquired the distribution of nonuniform stress and deformation of a three-dimensional model of a bolt-disk rotor. Li *et al.* [20] studied the dynamic model for the rotor system with the element and lumped mass modeling method, using the Newmark-ß method to analyze the system response. Xie *et al.* [21] analyzed the vibration characteristics with a rubbing–misalignment mixed fault of a dual-rotor system. Liu *et al.* [22] analyzed the frequency–amplitude characteristics of the flexible rotor system at high speed. Yu *et al.* [23] studied the influence of unbalance and rubbing on the rotor of the double-rotor system in a transient state. Arun *et al.* [24] adopted residual generation techniques to detect eccentricity and imbalance in the rotor-bearing model. Hsiao-Wei *et al.* [25] established FE models of the single rotor and double rotor and studied the dynamic behavior. Gao *et al.* [26] proposed a simplified two-rotor system to study the nonlinear dynamic characteristics of the system.

With the development of rotor dynamics, the rotor system is developing toward a higher rotation speed. The stability of the rotor system under high-speed operation is still the key and difficult point. Some of the above literature focuses on the dynamic behavior of a single rotor system, which is different from the actual aero-engine structure. Wang *et al.* [27] established a dynamic model of a dual-rotor system with unbalance and misalignment coupling faults. They employed numerical computational methods to calculate the vibration equations of the dual-rotor system and conducted unbalance experiments on a dual-rotor test rig. Gao *et al.* [28] developed a force model for shaft-axial bearings with localized defects on the outer or inner race surfaces. They utilized Lagrangian equations to establish the dynamic equations of the dual-rotor system and analyzed the nonlinear dynamics of shaft-axial bearings with localized defects. Yang *et al.* [29] utilized a hybrid beam-shell-spring element and model reduction method to consider rotational effects and constructed a FE model of a rotating-flexible shaft-disk-drum system with bolt connections. Ma *et al.* [30] combined FE methods with a free-interface modal synthesis method to establish a simplified dynamic model of a dual-rotor system. They particularly focused on analyzing the nonlinear dynamic behavior of a dual-rotor system supported by rolling bearings and squeeze film dampers (SFDs).For complex dual-rotor systems, the presence of inter-shaft bearings between the inner and outer rotors adds to the intricacy of rotor dynamics analysis and design due to the nonlinearities arising from bearing clearances and Hertz contact. Furthermore, in pursuit of enhanced operational capacity and efficiency, rotor systems, especially the inner rotors, are evolving toward higher speeds and slender configurations, often surpassing their minimum critical speeds. Presently, the prevailing support configuration for the high-speed, flexible inner rotor shaft in many dual-rotor systems typically adopts a three-point arrangement denoted as "1-1-1" or "0-2-1". In this paper, we will focus primarily on such a three-point support configuration.

In this paper, a coaxial dual-rotor system of "1-1-1" three-bearing support structure of high-speed flexible inner rotor is proposed according to the structure of the CFM56 aero-engine. On the basis of this model, the modeling method and dynamic characteristic analysis are studied. After designing a physical model with an inter-shaft bearing, the dynamic equation with unbalanced force is derived by applying the Newmark-ß method and Newton–Raphson method for numerical calculation. Then three different simulation models were designed for this study: beam-based FE (1D) model, solid-based FE (3D) model, and TM model. The modal frequencies and modal shapes in the static state are calculated, and the results of these three models were verified. The beam-based FE and TM models obtain the Campbell diagram and critical speeds. Finally, the effect of different disk unbalance phases and different speed ratios on the dynamic characteristics of the dual-rotor system is investigated in detail through unbalanced response analysis.

II. MODELING OF A COAXIAL DUAL-ROTOR SYSTEM

A. PHYSICAL MODEL

The CFM56 aero-engine is one of the most widely used aero-engines. As shown in Fig. 1(a), it has two independent rotor systems: inner (low-pressure) rotor and outer (high-pressure) rotor. The inner rotor contains a low-pressure (LP) compressor and LP turbine, while the outer rotor contains a high-pressure (HP) compressor and HP turbine. These two rotors were supported by five bearings support: support1, support2, support3, support4, and support5, and coupled by support 4.

Based on the structure of CFM56, this paper modeled a dual-rotor system, as shown in Fig. 1(b). Each rotor consists of a flexible shaft and two solid disks representing the compressor and turbine. The shaft of the inner rotor is solid, while the shaft of the outer rotor is hollow. The solid inner shaft, passing through the hollow outer shaft, is coupled by the inter-shaft bearing (roller bearing 4). The inner rotor is supported by deep groove ball bearing 1, roller bearing 2, and roller bearing 5, and the outer rotor is supported by deep groove ball bearing 3. Both inner and outer rotors can rotate independently in different directions and speeds, relying only on inter-shaft bearing 4 for motion coupling. Two-wheel disks (disk 1 and disk 4) are mounted on the inner rotor to represent the LP compressor and LP turbine, and other two-wheel disks (disk 2 and disk 3) are installed on the outer rotor to represent the HP compressor and HP turbine. The specific physical parameters used to describe the system are listed in Table I.

B. EQUATIONS OF MOTION

Based on the above physical model, the equation of motion of the dual-rotor system was established to study the dynamic characteristics by using the FE method. Timoshenko beam elements model the shaft, and the disk is regarded as lumped mass elements, shown in Figs. 2 and 3. Meanwhile, the model also considers the rotational inertia, gyroscopic effect, rotating shaft shear effect, and mass of the shaft and disk elements.

The Lagrange equation of motion is converted to obtain the differential equation of motion of the rigid disk and the flexible shaft element:
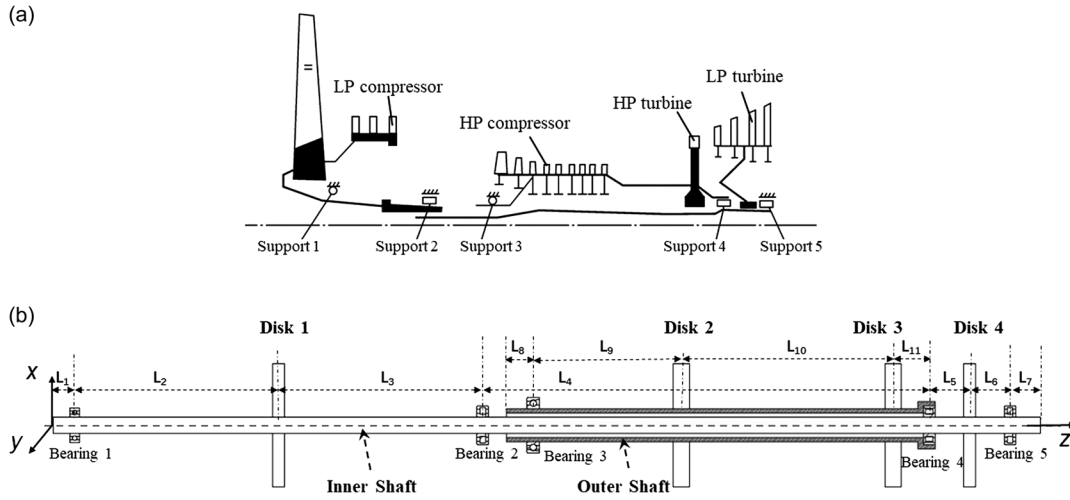
Fig. 1. Physical model: (a) the rotor-support structure of CFM56 and (b) the structural diagram of the dual-rotor system.

Table I. Model parameters of the dual-rotor system

Physical parameter	Value
Length of inner shaft Li (m)	1.2
Length of outer shaft Lo (m)	0.521
Outer and inner radii of inner shaft (m)	0.01,0
Outer and inner radii of outer shaft (m)	0.04,0.03
Elastic modulus of rotational shafts and disks (Pa)	2.06e11
Density of rotational shafts and disks (kg/m3)	7850
Poisson ratio of rotational shafts and disks	0.3
Length of inner shaft L1–L7 (m)	0.026,0.248,0.248,0.543,0.049,0.049,0.037
Length of inner shaft L8–L11 (m)	0.0325,0.180,0.2575,0.051
Mass property of disk 1 and disk 4 (kg)	2.031
Jd property of disk 1 and disk 4 (kg*m2)	2.856e-3
Jp property of disk 1 and disk 4 (kg*m2)	5.712e-3
Mass property of disk 2 and disk 3 (kg)	2.561
Jd property of disk 2 and disk 3 (kg*m2)	3.601e-3
Jp property of disk 2 and disk 3 (kg*m2)	7.203e-3
Bearing stiffness of bear 1 (N/m)	4.27e7
Bearing stiffness of bear 2 (N/m)	2.28e8
Bearing stiffness of bear 3 (N/m)	2.28e8
Bearing stiffness of bear 4 (N/m)	5.93e7
Bearing stiffness of bear 5 (N/m)	3.25e8
Unbalance mass (kg*m)	2.5E-5

$$\begin{cases} M_d \ddot{q}_{vd} + \Omega G_{qd} = F_{vd} \\ M_d \ddot{q}_{wd} - \Omega G_{vd} = F_{wd} \end{cases} \quad (1)$$

where $M_d = \begin{bmatrix} m \\ & J_d \end{bmatrix}$, $G = \begin{bmatrix} 0 \\ & J_p \end{bmatrix}$. M_d represents the mass matrix of the disk. m represents the mass of the disk. J_d represents the diameter moment of inertia. J_p represents the polar moment of inertia. Ω represents the angular velocity of disk rotation. G represents the gyroscopic matrix of the disk element. F_{vd} and F_{wd} represent the corresponding generalized forces:

$$\begin{cases} M_s \ddot{q}_{vs} + \Omega G_s \dot{q}_{ws} + K_s q_{vs} = F_{vs} \\ M_s \ddot{q}_{ws} - \Omega G_s \dot{q}_{vs} + K_s q_{ws} = F_{ws} \end{cases} \quad (2)$$

where M_s, K_s, G_s represent the mass matrix, stiffness matrix, and polar moment of inertia matrix of the shaft element, respectively. F_{vs} and F_{ws} represent the corresponding generalized forces, including unbalance force.

The motion differential equation of the inter-shaft bearing and the ordinary support assembly can be expressed as:

$$-C_b \dot{q}_b - K_b q_b = F_b \quad (3)$$
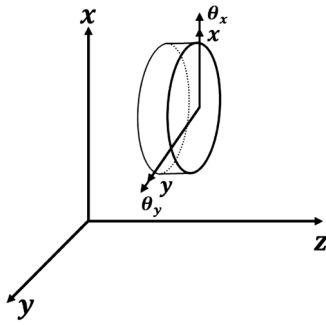
Fig. 2. Disk element.
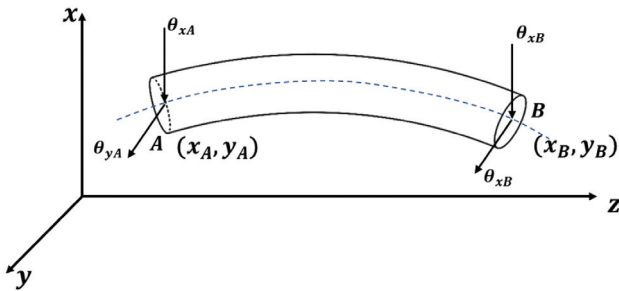
Fig. 3. Shaft element.

where C_b represents the bearing damping matrix. K_b represents the bearing stiffness matrix. q_b represents the bearing displacement and F_b marks the external bearing force. C_b and K_b can be written as:

$$C_b = \begin{bmatrix} c_{xx} & c_{xy} \\ c_{yx} & c_{yy} \end{bmatrix}, K_b = \begin{bmatrix} k_{xx} & k_{xy} \\ k_{yx} & k_{yy} \end{bmatrix}, c_{xx} = c_{yy},$$

$$k_{xx} = k_{yy}, c_{xy} = c_{yx} = 0, k_{xy} = k_{yx} = 0.$$

The independent differential equations of the dual-rotor system are divided into differential equations of the LP rotor and the HP rotor:

$$\begin{cases} M_l \ddot{q}_{vl} + \Omega_l G_l \dot{q}_{wl} + K_l q_{vl} = F_{vl} \\ M_l \ddot{q}_{wl} - \Omega_l G_l \dot{q}_{vl} + K_l q_{wl} = F_{wl} \end{cases} \quad (4)$$

where $q_{vl} = [\, x_1, \quad \theta_{x1}, \quad x_2, \quad \theta_{x2}, \quad \ldots \quad x_m, \quad \theta_{xm} \,]^{\mathrm{T}}$, $l = [\, y_1, \quad \theta_{y1}, \quad y_2, \quad \theta_{y2}, \quad \ldots \quad y_m, \quad \theta_{ym} \,]^{\mathrm{T}}$.

$$\begin{cases} M_h \ddot{q}_{vh} + \Omega_h J_h \dot{q}_{wh} + K_h q_{vh} = F_{vh} \\ M_h \ddot{q}_{wh} - \Omega_h J_h \dot{q}_{vh} + K_h q_{wh} = F_{wh} \end{cases} \quad (5)$$

where $q_{vh} = [\, x_{m+1}, \quad \theta_{x(m+1)}, \quad x_{m+2}, \quad \theta_{x(m+2)}, \ldots x_{m+n}, \theta_{x(m+n)} \,]^{\mathrm{T}}$, $q_{wh} = [\, y_{m+1}, \quad \theta_{y(m+1)}, \quad y_{m+2}, \theta_{y(m+2)}, \ldots y_{m+n}, \theta_{y(m+n)} \,]^{\mathrm{T}}$.

M_l and M_h represent the integrated mass matrices. $\Omega_l G_l$ and $\Omega_h G_h$ represent the integrated rotation matrices. K_l and K_h represent the integrated stiffness matrices. F_{vl}, F_{wl}, F_{vh}, and F_{wh} represent external excitation. m and n represent the total number of nodes of the LP and HP rotor system, respectively.

As shown in Fig. 4, when the rotor rotates around the point O_1 and at angular velocity Ω, the centrifugal force of the rotor disk mass eccentricity is F_u and the direction is outward along with OC. Points O and C are the center and center of mass of the disk, respectively:
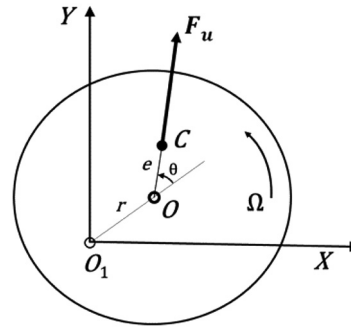
Fig. 4. Unbalance excitation vector.

$$F_u = m_d e \Omega^2 \quad (6)$$

Considering all the damping, stiffness, and mass matrices of the shaft, disk, and bearing, the general dynamic equation of the double-rotor system is

$$M\ddot{q} + (C + \Omega_l G_l - \Omega_h G_h)\dot{q} + Kq = F_u \quad (7)$$

where M, C, and K represent the mass matrix, damping matrix, and stiffness matrix of the dual-rotor system, respectively. q represents the displacement vector. Ω_l and G_h represent the speed. G_l and G_h represent the gyroscopic matrices. $\Omega_l G_l$ and $\Omega_h G_h$ represent the rotation matrices. F_u represents the unbalance excitation vector of the rotor system.

III. SIMULATION ANALYSIS AND DISCUSSIONS

A. SIMULATION MODELS

In this section, three different models of the dual-rotor system are modeled: beam-based FE model, solid-based FE model, and TM model. In order to analyze the dynamic characteristics of the dual-rotor system, the following assumptions were made in the discrete dynamics modeling process:

a) The disks of HP compressor, LP compressor, HP turbine, and LP turbine are all considered rigid disks with rotary effect. They are concentrated at the centroid position of the disk in the form of lumped mass and moment of inertia.

b) The shafts of the inner rotor and the outer rotor are simplified as annular beams with equal sections individually. The inner and outer shafts are Timoshenko beam elements without considering the influence of torsion and axial force.

c) Ignoring all the damping and the cross coefficient of the bearing, only the stiffness coefficients of the horizontal and vertical directions of the bearing are considered.

d) The inner and outer rotors rotate in the forward direction, with the outer rotor rotating 1.3 times the inner rotor.

1. BEAM-BASED FE MODEL. As illustrated in Fig. 5(a), the dual-rotor system is divided into several Timoshenko beam elements with nodes for building a 1D FE. The inner
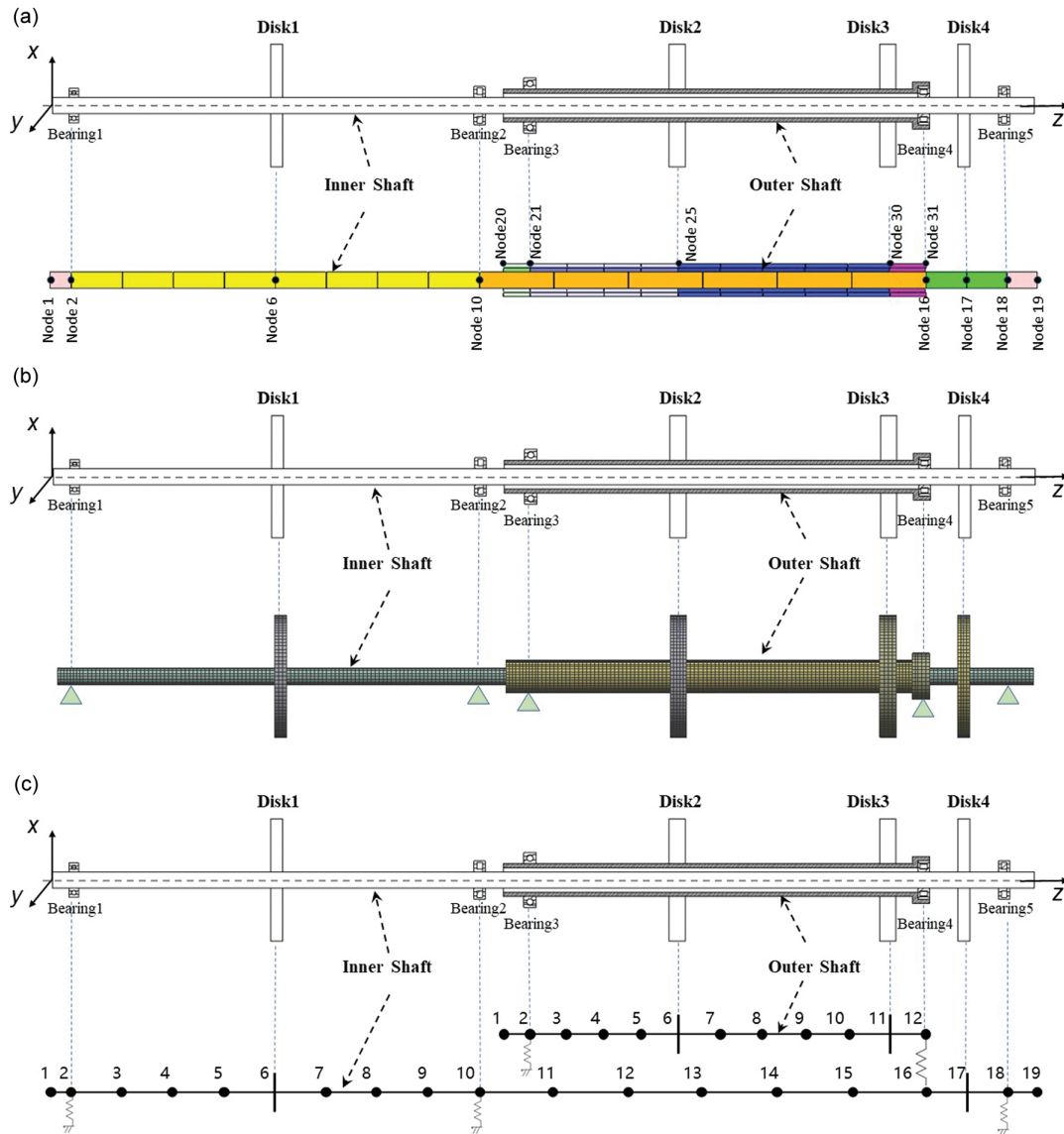
Fig. 5. Three models of the dual-rotor system: (a) beam-based FE model, (b) solid-based FE model, and (c) TM model.

rotor is modeled with 18 elements and 19 nodes. The outer rotor is modeled with 11 elements and 12 nodes. The bearings are assumed to be linear and isotropic. Bearing 1, bearing 2, bearing 3, and bearing 5 are located at nodes 2, 10, 21, and 18, respectively, while bearing 4 (the inter-shaft bearing) is located at node 16 and node 31. The rigid disk 1, disk 2, disk 3, and disk 4 are located at nodes 6, 25, 30, and 17.

2. SOLID-BASED FE MODEL. As illustrated in Fig. 5(b), a 3D solid-based model is established using the Ansys software package for the dual-rotor system. The inner rotor is discretized into 63020 hexahedral elements and 12690 nodes. The outer rotor is discretized into 76806 hexahedral elements and 14742 nodes.

3. TM MODEL. In the simulation of the TM model, this paper adopts the same parameter setting as the beam-based FE model, which mainly means that the number and position of nodes of inner and outer rotors remain the same after discretization. However, it is worth noting that the mass of the beam-based FE model is evenly distributed, while the beam in the TM model has no mass.

The simulation results of the above three numeric models are relatively consistent. In terms of calculation time, the solid-based FE model takes about 300 s, and the beam-based FE model and the TM model only take less than 1 s. The dual-rotor system's natural frequency varies with the dual-rotor system's speed. Then these two methods are more suitable for the application of real-time computing. Compared with the beam-based FE and TM models, both methods adopt the Timoshenko beam hypothesis when dealing with beam segments, and the shear stress and moment of inertia are considered. The TM model is simple to program and has the fastest calculation speed. However, it focuses on qualitative analysis, which is suitable for calculating the inherent characteristics of the dual-rotor system and is difficult to calculate the fault dynamics analysis. Although the beam-based FE model is complicated to program and occupies a large amount of memory, it is not worth mentioning in the face of modern computer technology. At the same time, the most significant advantage is elementary to expansion, especially the transient dynamic response, which is very important for the dual-rotor, real-time fault diagnosis system.

B. CALCULATION OF NATURAL FREQUENCY CHARACTERISTIC

Based on the above FE mathematical model and the three simulation models, the modal analysis of the dual-rotor system is carried out by using the MATLAB program, Ansys program, and TM program, respectively. TM program is solved by the Riccati method and programmed by the C programming language. The primary purpose is to calculate the natural frequencies and compare the validity of the three simulation models.

The beam-based FE model and TM model were used to calculate the first five order natural frequencies, and the solid-based FE model was used to calculate the first four order natural frequencies. The results in Figs. 6–8 list the modal shapes of the first four natural frequencies corresponding to each model. It can be seen that the vibration modes of each natural frequency are almost the same. The final calculation results are shown in Table II. The errors in the calculation results are all within 3%.

The simulation results of the above three numeric models are relatively consistent. In terms of calculation time, the solid-based FE model takes about 300 s, and the beam-based FE model and the TM model only take less than 1 s. The dual-rotor system's critical speed varies with the dual-rotor system's speed [1,2,31]. Then these two methods are more suitable for the application of real-time computing. Compared with the beam-based FE and TM models, both methods adopt the Timoshenko beam hypothesis when dealing with beam segments, and the shear stress and moment of inertia are considered. The TM model is simple to program and has the fastest calculation speed. However, it focuses on qualitative analysis, which is suitable for calculating the inherent characteristics of the dual-rotor system and is difficult to calculate the fault dynamics analysis. Although the beam-based FE model is complicated to program and occupies a large amount of memory, it is not worth mentioning in the face of modern computer technology. At the same time, the most significant advantage is elementary to expansion, especially the transient dynamic response, which is very important for the dual-rotor system real-time fault diagnosis system.

Fig. 6. The first four natural frequencies and natural modals (solid-based FE model).
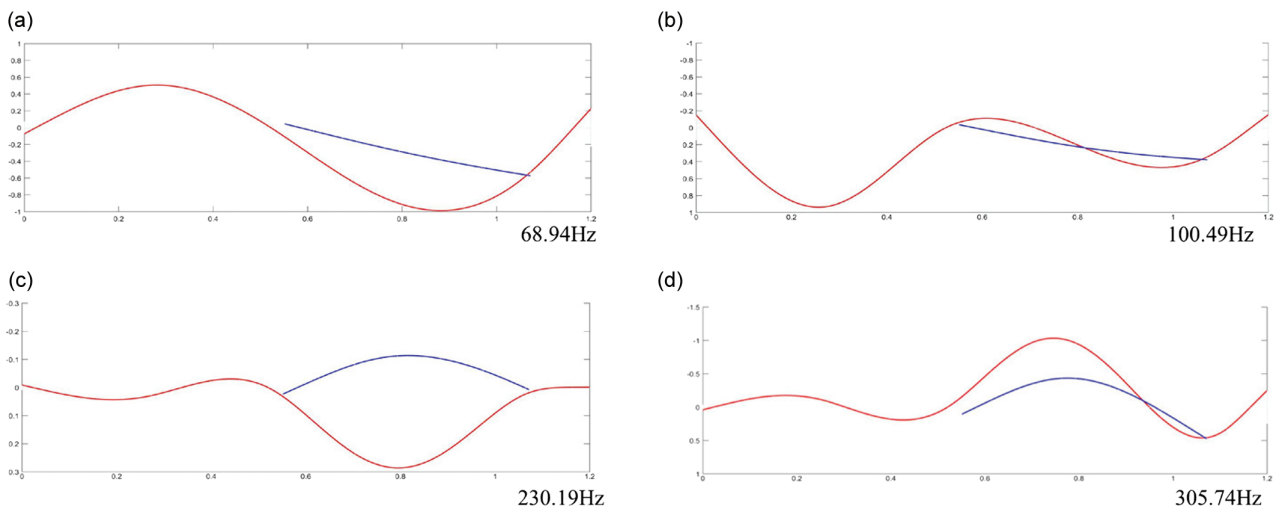
Fig. 7. The first four natural frequencies and natural modals (beam-based FE model).
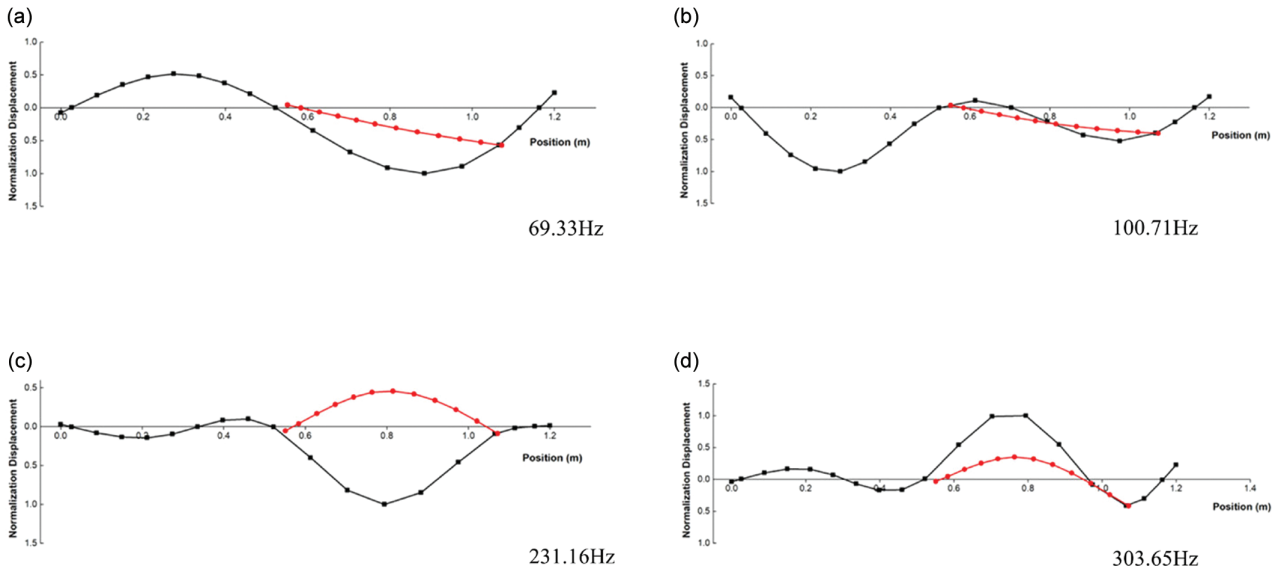
Fig. 8. The first four natural frequencies and natural modals (TM model).

Table II. Comparison of natural frequency components

Order	Beam-based FE model	Solid-based FE model	TM model	Error (%)
1	68.94	68.68	69.33	0.94
2	100.49	102.21	100.71	1.68
3	230.19	235.11	231.16	2.09
4	305.74	303.30	303.65	0.80
5	488.22	N/A	497.45	N/A

C. CALCULATION OF CRITICAL SPEED CHARACTERISTICS

The Campbell diagram is a diagram of the natural frequency and the rotational speed of the rotor system. For the dual-rotor system, each speed corresponds to a natural frequency. The Campbell diagram of the rotor system calculates the natural frequency of the whole system with one rotor as the primary excitation. While calculating the natural frequency, the inner and outer rotor speeds are, respectively, w1 and w2, and w2=1.3 w1. With the increase in rotor speed, the forward and reverse vortices corresponding to each frequency are not quite the same due to the gyroscopic effect. As shown in Fig. 9, solid line xFW and dotted line xBW represent the natural frequencies of forward vorticity and reverse vorticity, respectively. Therefore, first-order forward vorticity and reverse vorticity are represented as 1FW and 1BW, and so on. As mentioned above, the speed of the outer rotor in this paper is 1.3x that of the inner rotor, so the pink line represents the 1x synchronous excitation line of the inner rotor, and the brown line represents the 1.3x synchronous excitation line of the outer rotor. Therefore, the intersection points a, c, and e of the synchronous excitation line of the outer rotor and the forward vorticity line are the critical speeds of the dual-rotor system under the condition of the inner rotor acting as the primary excitation. The intersection points b and d of the synchronous excitation line of the inner rotor and the forward vorticity line are the critical speeds of the dual-rotor system under the condition of the outer rotor as
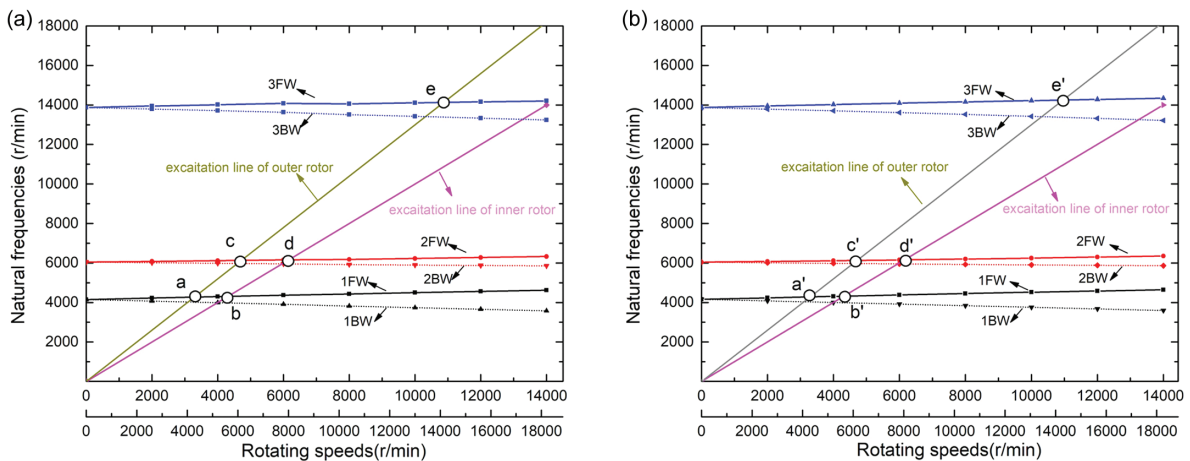
Fig. 9. Campbell diagram for the dual-rotor system: (a) Campbell diagram of beam-based FE model and (b) Campbell diagram of TM model.

Table III.   Comparison of first five critical speeds between beam-based FE model and TM model

Order	Beam-based FE model	TM model	Error (%)
First-order critical speed	a-(3289,4276)	a' -(3288,4281)	0.11
Second-order critical speed	b-(4319,5615)	b' -(4323,5634)	0.09
Third-order critical speed	c-(4721,6137)	c' -(4713,6132)	0.08
Fourth-order critical speed	d-(6168,8020)	d' -(6158,8005)	0.16
Fifth-order critical speed	e-(10860,14119)	e' -(10960,14250)	0.93
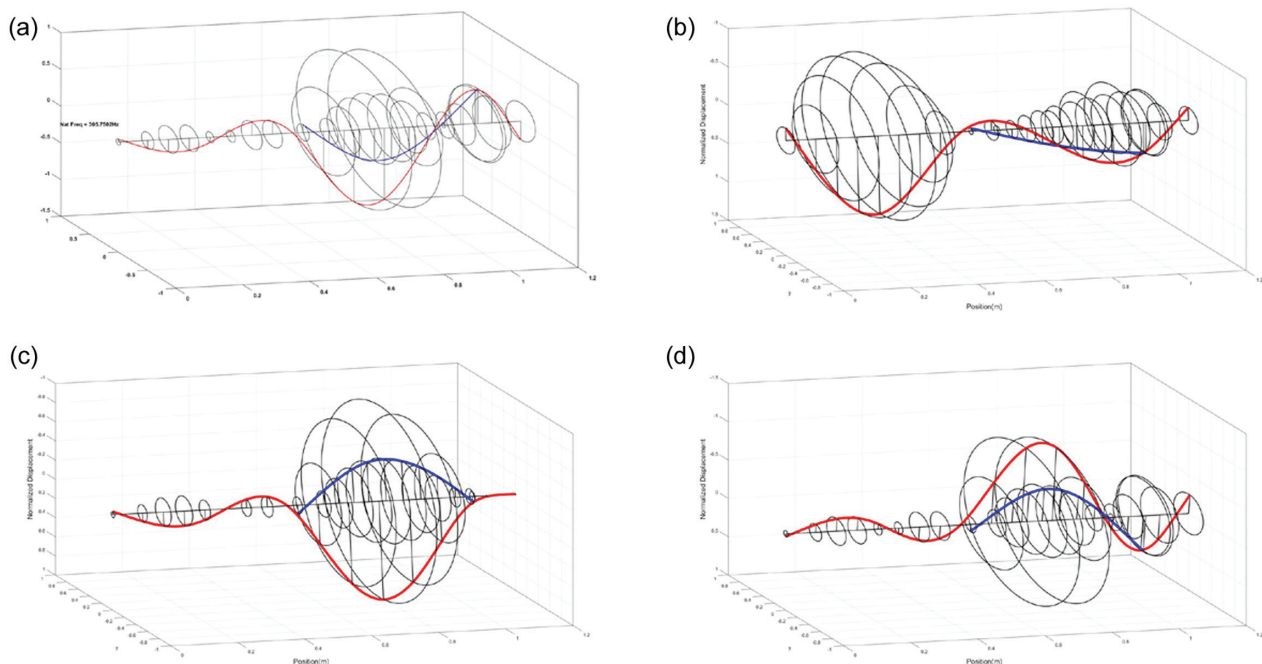
Fig. 10. MATLAB plots the first four critical speeds of the dual-rotor system.

the primary excitation. It can be seen from Table III that the errors of the critical speed calculation results between the beam-based FE model and TM model are within 1%. Of these five critical speeds, the second-order critical speed and the third-order critical speed are excited by the inner rotor and the outer rotor as the primary excitation, respectively. They are very close in numerical terms. The critical speed modes of the first four orders of the dual-rotor system are shown in Fig. 10. Hence, it will be probably a challenge to test these two critical speeds clearly in subsequent experiments.

D. UNBALANCED RESPONSE

The unbalanced response of the dual-rotor system is also studied in this paper to learn more dynamic characteristics of the dual-rotor system. This paper mainly studies the unbalanced response of inner rotor disks 1 and 4 and outer rotor disks 2 and 3 when the unbalances are in-phase and antiphase, respectively, shown in Fig. 11. At the same time, the unbalanced responses of inner and outer rotors with different speed ratios are also studied.

As illustrated in Fig. 12, the first two pictures respectively show the excitation of the inner rotor and the outer rotor with in-phase unbalances. The last two pictures respectively show the excitation of the inner rotor and

the outer rotor with antiphase unbalances. Furthermore, the speed ratio between the outer and inner rotor of the four groups of figures are ratio 1.3, ratio1.5, ratio1.8, and ratio2.2. The amplitudes of the four bearings have evident peak values at each critical speed, which correspond to the critical speed calculated in Table III.

Figure 13 shows the bearing vibration state of the excitation of the outer rotor with in-phase unbalances. Whether internal rotor excitation or the external rotor excitation, bearing 3 of the third critical speed has the most extensive vibration, while bearing 1 of the first and second critical speed has the most extensive vibration. Therefore, bearing 1 and bearing 3 are the best monitoring locations, providing theoretical support for the monitoring system construction of the test rig.

As previously introduced, bearing 1 has the most extensive vibration at the first and second critical speed, and bearing 3 has the most extensive vibration at the third critical speed. Therefore, the vibration amplitude at different speeds is taken out to obtain the Rate-Response amplitude diagram of bearing 1 in Fig. 14(a) and (b) at the first and second peaks and the Rate-Response amplitude diagram of bearing 3 in Fig. 14(c) at the third critical peak. As can be seen from these three figures, bearing 3 has the maximum vibration amplitude at the third peak point when the speed ratio is 1.3. Bearing 1 and 2 have the maximum
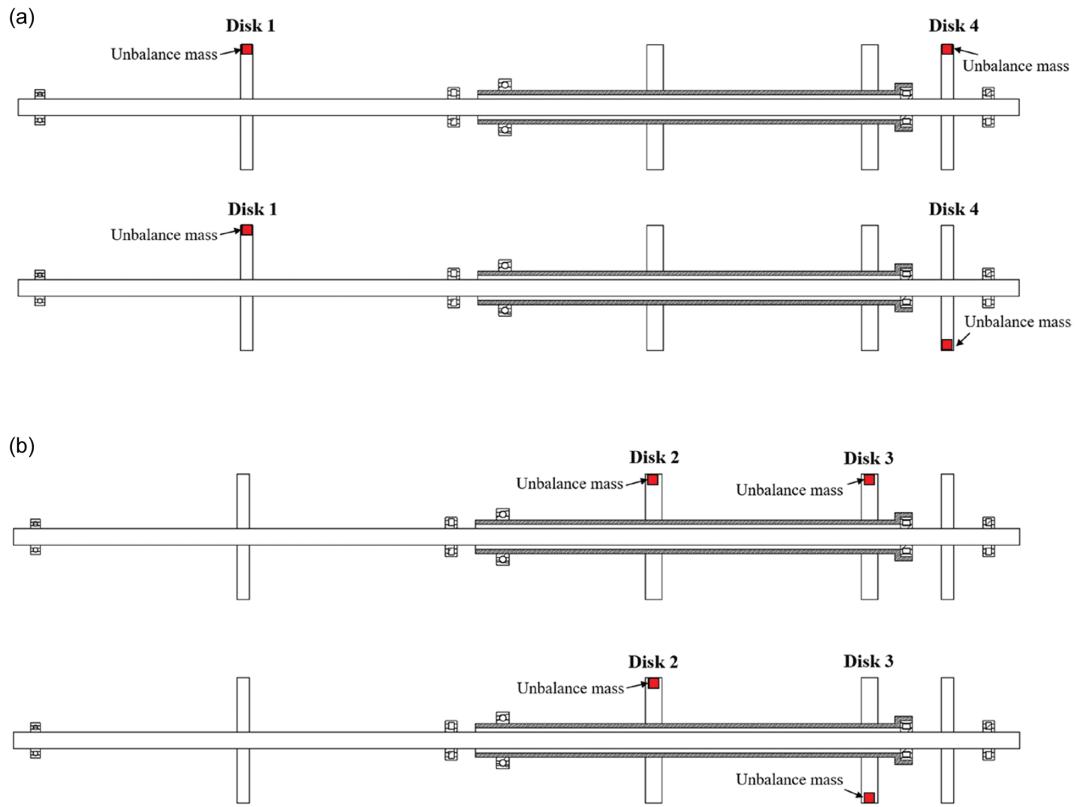
Fig. 11. Unbalanced position distribution: (a) in-phase and antiphase unbalance between disk 1 and disk 4 and (b) in-phase and antiphase unbalance between disk 2 and disk 3.
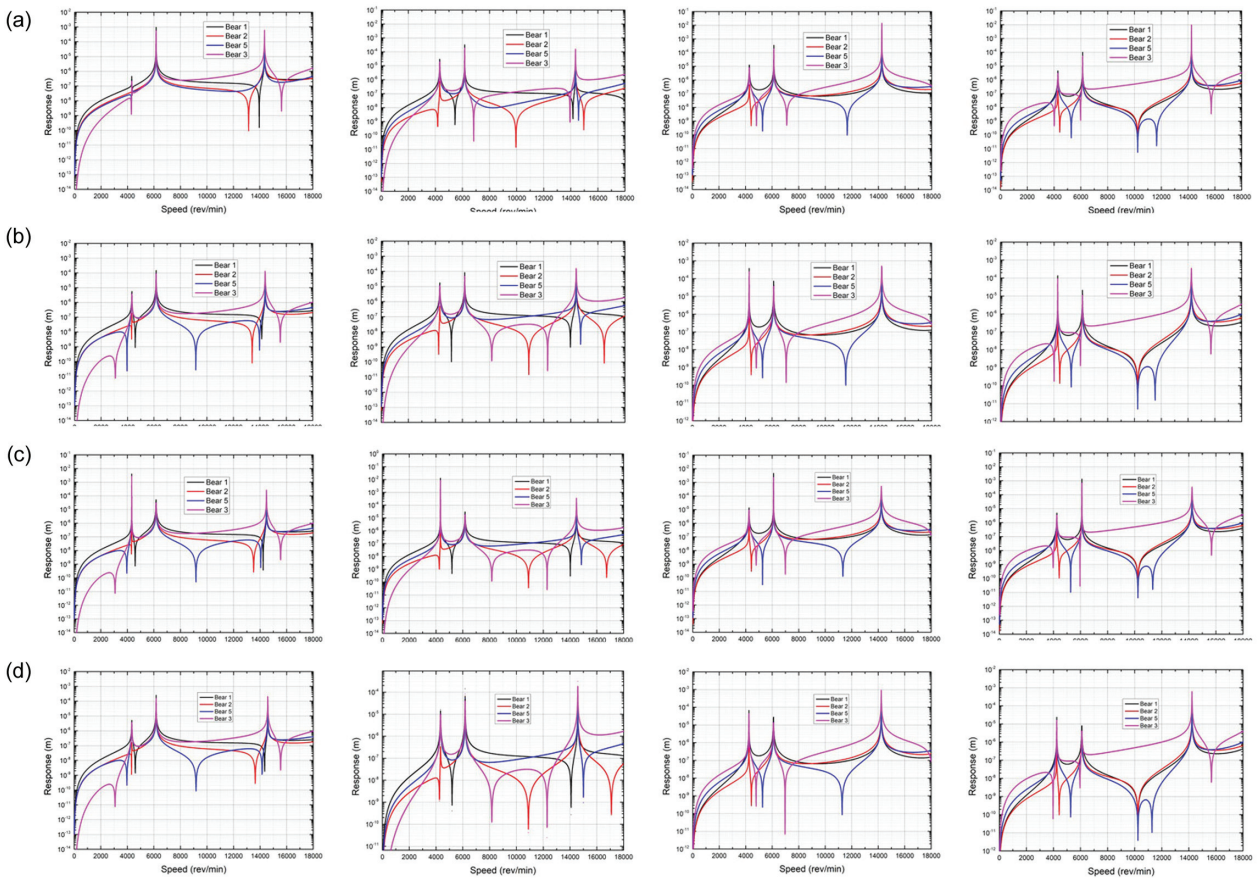
Fig. 12. The unbalanced response of dual-rotor system: (a) ratio = 1.3, (b) ratio = 1.5, (c) ratio = 1.8, and (d) ratio = 2.2.
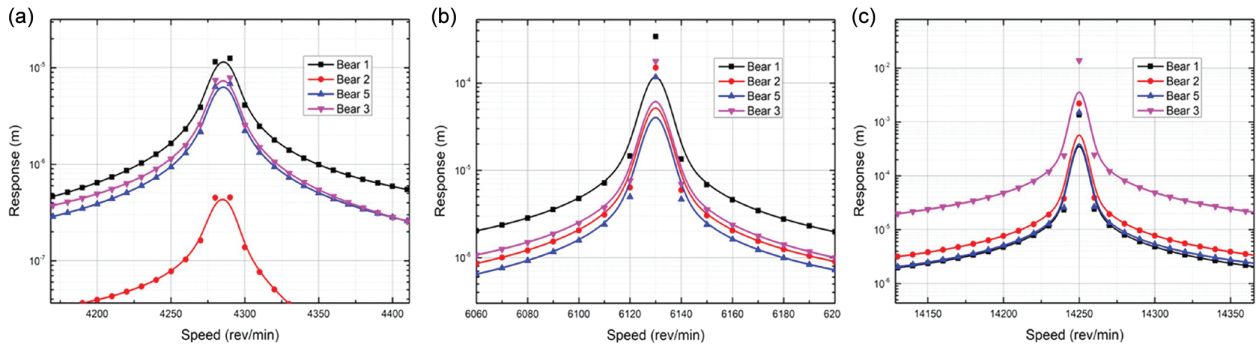
Fig. 13. Bearing vibrations amplitude.
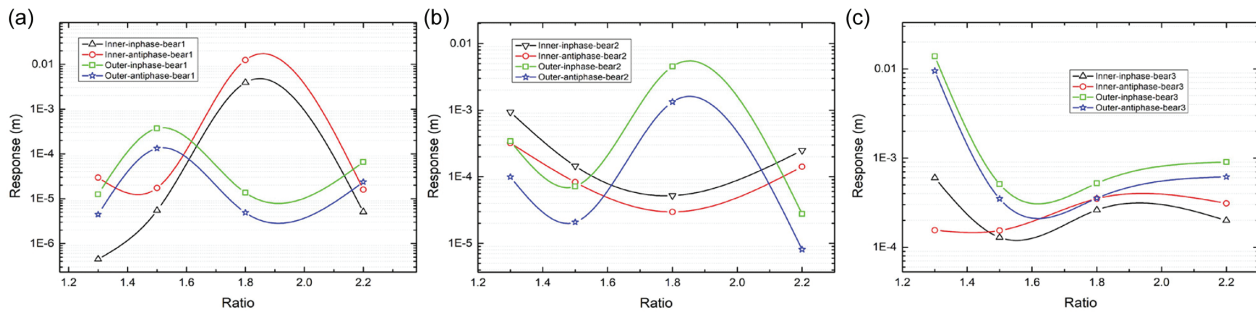
Fig. 14. Bearing 1, bearing 2, and bearing 3 vibrations at different ratios.

vibration amplitude at the first and second peak points when the speed ratio is 1.8. Therefore, setting different operating speed ratios plays an essential role in the stable operation of the aero-engine in engine design.

The ratio of antiphase unbalance amplitude to in-phase unbalance amplitude is amplitude ratio. In order to study the orientation effect of unbalance, the amplitude ratios between the in-phase and antiphase unbalance at different speed ratios in Table IV are presented. When the amplitude ratio is greater than 1, the unbalanced response with the in-phase unbalances is higher than with the antiphase. For less than 1, it is the opposite. Therefore, it can be seen from the table that the unbalanced response of the in-phase and antiphase excitation of the inner rotor is 65.842 at the maximum and 0.260 at the minimum, and some amplitude ratios are greater than 1, while others are less than 1. However, the unbalanced response of the in-phase and antiphase excitation of the outer rotor almost changes little with the speed rate change at each critical speed. The outer rotor is less affected by the in-phase and antiphase unbalance excitation, while the inner rotor is easily affected. It can be seen from the structure that the outer rotor has a small length-to-diameter ratio and a large stiffness, so it is not easily affected by unbalance. The length-to-diameter ratio of the inner rotor is sizeable, and the stiffness is small, so it

is easily affected by unbalance. The above analysis further indicates that the inner rotor should be focused on the dynamic behavior of the two-rotor system. It can be seen from the first three columns of Table IV that the unbalanced inversion promotes the dynamic vibration behavior at the first and third critical speeds while inhibiting the dynamic vibration behavior at the second critical speeds. At the rate of 1.3, the effect of the unbalance on vibration is volatile, which is also of great concern.

E. EXPERIMENT VERIFICATION

In order to verify the validity of the above model and results, this paper designed a dual-rotor system test rig. Figure 15 shows that the test rig mainly consists of the inner rotor assembly and outer rotor assembly. The inner rotor assembly is directly connected to the inner rotor shaft by the inner rotor motor through the spring coupling. As the above model is introduced, the inner rotor shaft mainly comprises bearing 1, bearing 2, bearing 5, disk 1, and disk 4. The drive shaft assembly is designed as the external sub-shaft cannot be driven directly by the motor, as shown in Fig. 15(b). The driving shaft assembly comprises the driving shaft, driving shaft lug, two supporting bearings, and related components. The driveshaft is also hollow and passes through the inner

Table IV.   Comparison of amplitude ratios between the in-phase and antiphase unbalance

Speed ratio	Inner-peak1	Inner-peak2	Inner-peak3	Outer-peak1	Outer-peak 2	Outer-peak 3
1.3	65.842	0.344	0.260	0.358	0.291	0.686
1.5	3.180	0.571	1.196	0.358	0.291	0.68586
1.8	3.200	0.569	1.341	0.359	0.293	0.68041
2.2	3.150	0.568	1.557	0.359	0.292	0.68195
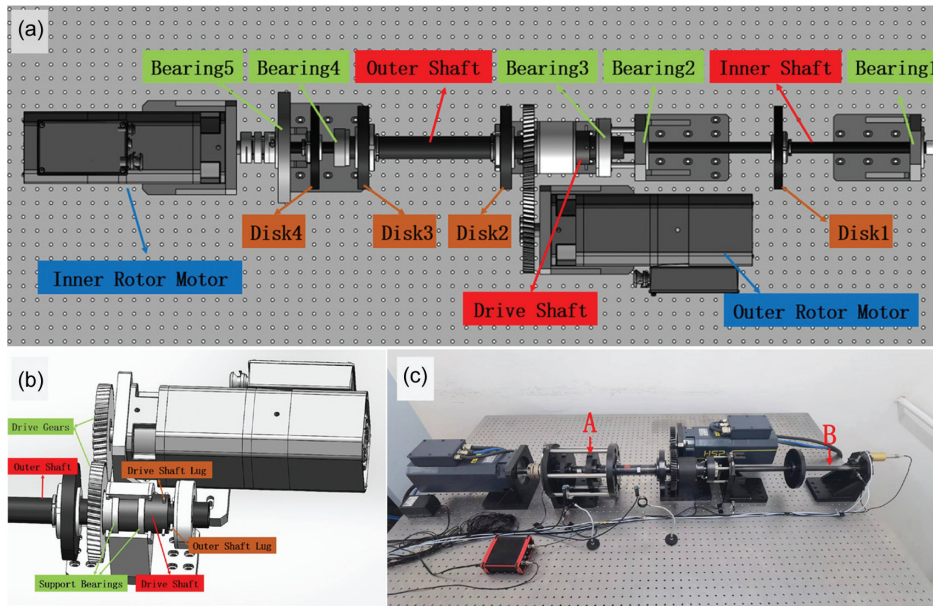
Fig. 15. Dual-rotor system test rig: (a) overall view, (b) drive part view, and (c) measure and excitation position.

rotor shaft and is supported by two support bearings. The external rotor motor can transfer the driving force through the drive gear to make the drive shaft rotate. The driving shaft and the inner rotor are provided with four lugs connected by soft, thin wires. In this way, the drive shaft can transfer torque through the four pairs of soft, thin lines without any other direction of force, thus driving the inner rotor rotation. The motor of the test rig has a rated power of 2.2 KW, a maximum speed of 10000 rpm, and a speed accuracy of ±2 rpm.

Experimental modal analysis of the test rig's inner rotor shaft system was conducted using the hammer impact method. As illustrated in Fig. 15(c), a force hammer was positioned at fixed point A, while a vibration sensor was placed at fixed point B to measure the rotor's vibration acceleration signals. By striking the rotor along the vertical direction and capturing the time–domain response curves via the acceleration sensor, as depicted in Fig. 16(a), the collected vibration signals underwent frequency spectrum analysis. After fast Fourier transform (FFT) processing, frequency–domain response curves were obtained, as depicted in Fig. 16(b). The results indicate that only the first-mode frequency of 66.5 Hz was excited during the experiment. This finding closely matches the natural frequencies

obtained from the preceding simulation model, which were 68.68 Hz, 68.94 Hz, and 69.33 Hz. Therefore, the experimental results validate the accuracy of the simulation models.

IV. CONCLUSION

In this paper, a dual-rotor system with a high-speed flexible inner rotor "1-1-1" three bearing support structure is modeled to study the modeling method and dynamic characteristics. Based on the dual-rotor physical model, a FE model with unbalanced force is designed by using the Timoshenko beam elements. After three different simulation models were designed, the modal frequencies, modal shapes, and critical speed characteristics were calculated. The unbalanced response of the system under unbalanced excitation was studied. The main conclusions are summarized as follows:

1) The natural frequency error rate calculated by the beam-based FE model, solid-based FE model, and TM model is less than 3%. The critical speed based on FE and TM is verified, proving the established model's effectiveness. The results show that the
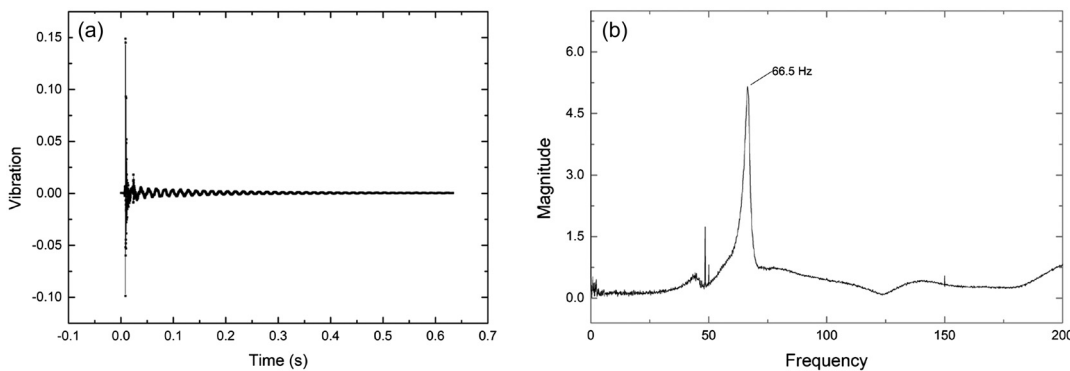
Fig. 16. Experiment results: (a) time–domain diagram of vibration signal and (b) spectrum diagram of vibration signal.

beam-based FE model has a very high computational speed and is elementary to expand for further dynamic research. These advantages are very suitable for studying the rotor system real-time fault diagnosis system.

2) The unbalanced response of the dual-rotor system is not linear but has a great relationship with the speed ratio. When the speed ratio is 1.8, the vibration amplitude of the first and second critical speeds is the largest. When the speed ratio is 1.3, the vibration amplitude of the third critical speed of the rotor system is the largest. Attention should be paid to designing the dual-rotor system.

3) The in-phase or antiphase unbalance mass affects the bearing vibration when the inner rotor is excited, but the outer rotor excitation does not. The reason is that the inner rotor has a sizeable length-to-diameter ratio, and the stiffness is minor, while the outer rotor has a relatively large stiffness. Therefore, compared with the outer rotor, the dynamic balance of the inner rotor is more critical, which will affect the stability of the whole system.

Based on the above study, further research about the dynamics of unbalanced force is of great significance in fault diagnosis and prognosis of the dual-rotor system. The modal experiment validates the simulated results, and further experiments will be conducted to confirm their validity.

CONFLICT OF INTEREST STATEMENT

REFERENCES

[1] Y. Zhong, Y. He, Z. Wang, and F. Li. *Rotor Dynamics*. Beijing: Tsinghua University Press, 1987.

[2] Z. Wang. *Rotor Dynamics Design for Rotating Machinery*. Beijing: Tsinghua University Press, 2015.

[3] R. L. Ruhl, T. F. Conry, and R. L. Steger, "Unbalanced response of a large rotor-pedestal-foundation system using an elastic half-space soil model," *J Mech Des N Y*, vol. 102, no. 2, pp. 311–319, 1980.

[4] H. D. Nelson and J. M. McVaugh, "The dynamics of rotor-bearing systems using finite elements," *Journal of Engineering for Industry*, vol. 98, no. 2, pp. 593–600, 1976.

[5] D. H. Hibner, "Dynamic response of viscous-damped multi-shaft jet engines," *J. Aircr.*, vol. 12, no. 4, pp. 305–312, 1975.

[6] N. Wang, D. Jiang, and H. Xu, "Dynamic characteristics analysis of a dual-rotor system with inter-shaft bearing," *Proceedings of the Institution of Mechanical Engineers, Part G: Journal of Aerospace Engineering*, vol. 233, no. 3, pp. 1147–1158, 2019.

[7] N. Wang, C. Liu, D. Jiang, and K. Behdinan, "Casing vibration response prediction of dual-rotor-blade-casing system with blade-casing rubbing," *Mech. Syst. Sig. Process.*, vol. 118, no. 2, pp. 61–77, 2019.

[8] N. Wang and D. Jiang, "Vibration response characteristics of a dual-rotor with unbalance-misalignment coupling faults: theoretical analysis and experimental study," *Mech. Mach. Theory*, vol. 125, pp. 207–219, 2018.

[9] N. Wang, C. Liu, and D. Jiang, "Experimental analysis of dual-rotor-support-casing system with blade-casing rubbing," *Eng. Fail. Anal.*, vol. 123, p. 105306, 2021.

[10] L. Wang, A. Wang, M. Jin, Y. Yin, X. Heng, and P. Ma, "Nonlinear dynamic response and stability of a rod fastening rotor with internal damping effect," *Arch. Appl. Mech.*, vol. 91, no. 9, pp. 3851–3867, 2021.

[11] L. Wang, A. Wang, M. Jin, Q. Huang, and Y. Yin, "Nonlinear effects of induced unbalance in the rod fastening rotor-bearing system considering nonlinear contact," *Arch. Appl. Mech.*, vol. 90, no. 5, pp. 917–943, 2020.

[12] M. H. Jalali, M. Ghayour, S. Ziaei-Rad, and B. Shahriari, "Dynamic analysis of a high speed rotor-bearing system," *Measurement*, vol. 53, pp. 1–9, 2014.

[13] W. Yang, M. Liang, L. Wang, and H. Yuan, "Research on unbalance response characteristics of gas turbine blade-disk rotor system," *Journal of Vibroengineering*, vol. 20, no. 4, pp. 1676–1690, 2018.

[14] Y. Yang, Y. Yang, D. Cao, G. Chen, and Y. Jin, "Response evaluation of imbalance-rub-pedestal looseness coupling fault on a geometrically nonlinear rotor system," *Mech. Syst. Sig. Process.*, vol. 118, pp. 423–442, 2019.

[15] Y. Yang, "Response analysis of a dual-disc rotor system with multi-unbalances–multi-fixed-point rubbing faults," *Nonlinear Dyn.*, vol. 87, pp. 109–125, 2017.

[16] Z.-X. Fei, S.-G. Tong, and C. Wei, "Investigation of the dynamic characteristics of a dual rotor system and its start-up simulation based on finite element method," *Journal of Zhejiang University SCIENCE A*, vol. 14, no. 4, pp. 268–280, 2013.

[17] Z. Lu, S. Zhong, H. Chen, Y. Chen, J. Han, and C. Wang, "Modeling and dynamic characteristics analysis of blade-disk dual-rotor system," *Complexity*, vol. 2020, no. 4, pp. 1–13, 2020.

[18] Y. Jin, Z. Liu, Y. Yang, F. Li, and Y. Chen, "Nonlinear vibrations of a dual-rotor-bearing-coupling misalignment system with blade-casing rubbing," *J. Sound Vib.*, vol. 497, p. 115948, 2021.

[19] H. Zhang, Y. Liu, and X. Huang, "Nonlinear dynamic performance of a bolt-disc rotor with the position error of circumferential bolt-holes," *Shock Vib.*, vol. 2021, pp. 1–10, 2021.

[20] Y. Li, Z. Luo, J. Liu, H. Ma, and D. Yang, "Dynamic modeling and stability analysis of a rotor-bearing system with bolted-disk joint," *Mech. Syst. Sig. Process.*, vol. 158, p. 107778, 2021.

[21] W. Xie, C. Liu, N. Wang, and D. Jiang, "Numerical and experimental analysis of rub-bing–misalignment mixed fault in a dual-rotor system," *Proceedings of the Institution of Mechanical Engineers, Part C: Journal of Mechanical Engineering Science*, vol. 235, pp. 3179–3198, 2020.

[22] J. Liu, C. Tang, and G. Pan, "Dynamic modeling and simulation of a flexible-rotor ball bearing system," *J. Vib. Control*, vol. 28, no. 23–24, p. 15.

[23] P. Yu, "Dynamic modeling and vibration characteristics analysis of the aero-engine dual-rotor system with Fan blade out," *Mech. Syst. Sig. Process.*, vol. 106, pp. 158–175, 2018.

[24] A. K. Jalan and A. R. Mohanty, "Model based fault diagnosis of a rotor–bearing system for misalignment and unbalance under steady-state condition," *J. Sound Vib.*, vol. 327, no. 3–5, pp. 604–622, 2009.

[25] H.-W. D. Chiang, C.-N. Hsu, and S.-H. Tu, "Rotor-bearing analysis for turbomachinery single- and dual-rotor systems," *J. Propul. Power*, vol. 20, no. 6, pp. 1096–1104, 2004.

[26] P. Gao, L. Hou, R. Yang, and Y. Chen, "Local defect modelling and nonlinear dynamic analysis for the inter-shaft bearing in a dual-rotor system," *Appl. Math. Modell.*, vol. 68, pp. 29–47, 2019.

[27] N. Wang and D. Jiang, "Vibration response characteristics of a dual-rotor with unbalance- misalignment coupling faults: theoretical analysis and experimental study," *Mech. Mach. Theory*, vol. 125, pp. 207–219, 2018.

[28] P. Gao, L. Hou, R. Yang, and Y. Chen, "Local defect modelling and nonlinear dynamic analysis for the inter-shaft bearing in a dual-rotor system," *Appl. Math. Modell.*, vol. 68, pp. 29–47, 2019.

[29] T. Yang, H. Ma, Z. Qin, H. Guan, and Q. Xiong, "Coupling vibration characteristics of the shaft-disk-drum rotor system with bolted joints," *Mech. Syst. Sig. Process.*, vol. 169, p. 108747, 2022.

[30] X. Ma, H. Ma, H. Qin, X. Guo, and M. Yu, "Nonlinear vibration response characteristics of a dual-rotor-bearing system with squeeze film damper," *Chin. J. Aeronaut.*, vol. 34, no. 10, pp. 128–147, 2021.

[31] S. Huaitao, Z. Jizong, Z. Yu, and H. Gang, "Calculation and analysis of critical speed of high speed motor spindle rotor system," *IOP Conference Series: Materials Science and Engineering*, vol. 399, no. 1, p. 012025, 2018.